Layer-dependent dielectric modulation in WS_2/GaN heterostructures

Weiqing Tang [*], Zongnan Zhang [*], Hao Zeng, Yaping Wu [†], Zhiming Wu [‡], Xu Li, Chunmiao Zhang, and Junyong Kang
Department of Physics, Engineering Research Centre for Micro-Nano Optoelectronic Materials and Devices at Education Ministry, Fujian Provincial Key Laboratory of Semiconductor Materials and Applications, Xiamen University, Xiamen, 361005, People's Republic of China

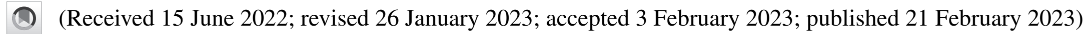
(Received 15 June 2022; revised 26 January 2023; accepted 3 February 2023; published 21 February 2023)

Controlling over the electronic structure of two-dimensional (2D) semiconductors is crucial to unlock their full potential in the applications in future nanodevices. Here, we demonstrate a layer-dependent dielectric modulation of electronic structures in multilayer WS_2/GaN heterostructures. The results investigated by means of *in situ* scanning tunneling microscopy/spectroscopy and photoluminescence spectroscopy show that the fluctuations of the dielectric environment induced by local corrugation of the GaN surface dramatically tune the band structure of monolayer WS_2 with a large downshift of the valence band maximum by about 1.12 eV. Under the shielding effect of the first-layer WS_2, the dielectric environment shows a weak modulation effect on the second-layer, and even has negligible influence on the third- and fourth-layer WS_2. The relationship between dielectric environment and interfacial distance is further simulated through first-principles calculations. The electrostatic potential energy, differential charge densities, and charge transfer of the WS_2/GaN heterostructure under different interfacial distances reveal that the differences of charge redistributions between the WS_2/GaN interface and WS_2 interlayer are responsible for the layer-dependent dielectric modulation. This work offers some references for the design and fabrication of novel 2D optoelectronic devices.

DOI: 10.1103/PhysRevB.107.085304

I. INTRODUCTION

Understanding of the electronic structure and electron-matter interactions in quantum regimes is an extremely active and advanced research field that has driven remarkable progress from fundamental science to practical application of materials [1–3]. For the atomically thin two-dimensional (2D) semiconductors, quantum confinement and reduced dielectric screening could enhance Coulomb interaction between carriers, leading to a significant renormalization of the electronic structure [4–6]. Since the screening effect is intensively dependent on the immediate surroundings (vacuum, air, or substrate) of materials [7–11], the Coulomb interaction between carriers is dramatically sensitive to the local dielectric environment, as demonstrated in theoretical calculations of environmental screening [12,13] and in measured changes of the exciton Bohr radius [14]. Correspondingly, the quasiparticle band gap of 2D materials can be modified by local changes in the external dielectric environment, which allow for noninvasive construction and engineering of lateral heterostructures using the same material [15]. Semiconducting transition-metal dichalcogenides (TMDs), such as WS_2, are typical 2D materials with remarkable electronic properties [8,16]. It has been demonstrated that the variation of the band gap for monolayer (ML) TMDs induced by the external dielectric environment can reach the order of hundreds of millielectronvolts with respect to that of freestanding materials [3,10,14,17]. Meanwhile, the effective control of the dielectric effect in 2D TMDs is an issue of concern that determines device performance. It has been reported that the inhomogeneous dielectric environment, i.e., dielectric disorder, could be shielded through constructing van der Waals heterostructures, such as being encapsulated by hexagonal BN (h-BN) and contacting with graphene [18,19].

Substrate is an important dielectric environment for 2D materials. Spatial corrugation, surface adsorbates, and the polarization field of the substrate will lead to a variation in the dielectric effect surrounding materials [20]. Recent reports involving the use of optical measurements show the modulation of exciton state energies and band gaps of ML WS_2 and WSe_2 by the dielectric environment of substrates [18,21,22]. An exciton resonance broadening of ∼20 meV was found on polydimethylsiloxane and the h-BN surface, while a large variation of the band gap and exciton binding energy ranging up to 100 meV was modulated by SiO_2/Si [18]. Nevertheless, an overlap of the band-edge absorption step with strong excitonic resonances generally makes it challenging to determine the band structure of 2D semiconductors accurately from the optical measurements [23]. Consequently, a study from the electronic aspect is necessary. Scanning tunneling microscopy (STM) is a versatile and efficient tool to study the electronic structure of 2D semiconductors [24], and is capable of investigating the local dielectric modulation effects induced by the substrate at the atomic scale. III-nitrides with a tunable band gap have been widely applied in electronics and optoelectronics [25]. Their strong surface polarization fields could be considered functionalized dielectric environments for modulating the electronic structure and electron-matter interactions in 2D materials. Among the III-nitrides, GaN possesses the lattice constant well matched that of WS_2 [26,27], providing a favorable platform for the fabrication of an integrated

[*]These authors contributed equally to this work.
[†]Corresponding author: ypwu@xmu.edu.cn
[‡]Corresponding author: zmwu@xmu.edu.cn

 ©2023 American Physical Society

heterostructure with WS_2 to ascertain the dielectric modulation. In addition, the dielectric modulation and disorder screening effects on the electronic structures will be thickness dependent for 2D layered materials, which will offer an additional layer of freedom for controlling material properties. The intrinsic physical mechanism is of significant importance, and has not yet been reported.

Herein, high-quality WS_2 films with MLs, bilayer (BLs), trilayer (TLs), and four layers (FLs) are controlled-synthesized on a GaN substrate through chemical vapor deposition (CVD). Low-temperature STM is employed to characterize the surface topography and electronic structure for WS_2/GaN heterostructures with different WS_2 thickness. By combining scanning tunneling spectroscopy (STS), photoluminescence (PL) measurements, and first-principles calculations, the band alignments between the GaN and WS_2 layers, dielectric modulation from the GaN substrate, and the layer-dependent dielectric screening effect of WS_2 are revealed. Differential charge densities and electrostatic potential energies are calculated to analyze the physical mechanism of the layer-dependent dielectric effect for WS_2/GaN heterostructures.

II. METHODS AND CHARACTERIZATION

Two-dimensional WS_2 layers are synthesized on N-polar GaN substrates through our developed method, which combines CVD and thermal evaporation [28]. Sulfur (Aladdin, 99.99%) powder and a deposited WO_3 (Alfa Aesar, 99.9%) film on a SiO_2/Si slice are employed as the precursors. The thickness of the WO_3 film is well adjusted to control the growth thickness of the WS_2 layers [28]. Morphologies of the WS_2/GaN heterostructures are characterized by a FEI Quanta-600 FEG Environmental scanning electron microscope with a beam voltage of 10 kV. Raman and PL spectra are recorded using a 532-nm excitation laser combined with a 100× objective in a Horiba LabRam HR Evolution confocal spectrometer. The power of the excitation laser is ∼3 mW, and the beam size is ∼1 μm. All STM investigations reported here are acquired using chemically etched tungsten tips in constant-current mode at a cryogenic temperature of about 78 K and a base pressure of about 6×10^{-11} torr [29]. The WS_2/GaN heterostructures are annealed under ultrahigh-vacuum conditions at 573 K for 16 h to achieve a clean surface before the STM measurements are made. STS is conducted using the standard lock-in technique with a modulation signal of 10 mV peak-to-peak at 957 Hz.

The first-principles calculations are performed in the Vienna Ab initio Simulation Package by using density functional theory (DFT) with the projector augmented wave pseudopotential [30]. The 1 × 1 slab models with 30−Å vacuum layers along the Z direction are constructed to simulate the WS_2/GaN heterostructures. The exchange-correlation effects are treated by the generalized gradient approximation of Perdew-Burke-Ernzerhof [31]. The dispersion-corrected density functional theory (DFT-D2) method is used to describe the van der Waals interaction between WS_2 and GaN. The 2D Brillouin zone is sampled with a 11 × 11 × 1 Monkhorst-Pack grid of k−points, and the truncation of plane-wave energy is set to 364 meV [32]. All the atomic degrees of freedom are fully relaxed with self-consistent convergence criteria of 10^{-4} eV and 0.01 eV Å^{-1} for total energy and Hellmann-Feynman forces, respectively.

III. RESULTS AND DISCUSSION

The electronic morphology of the GaN surface is characterized and shown in Supplemental Material Fig. S1 [33]. The step-like and spiral hillock-like structures are observed on the GaN surface, which are similar to other reports [34,35]. The morphology of as-grown WS_2 on the GaN substrate exhibits uniform triangular islands with the domain size at the microlevel, as observed in the scanning electron microscopy (SEM) image in Fig. 1(a). Figure 1(b) displays the Raman spectrum of the WS_2/GaN heterostructure, in which four Raman peaks are located at 358.3, 420.5, 570.7, and 736.5 cm^{-1}, respectively. The first two peaks are assigned to the in-plane (E_g) and out-of-plane (A_g) vibrational modes of WS_2, respectively. From their frequency separation of ∼62 cm^{-1} [36], the few-layer structure of the film is demonstrated. The other two peaks are identified as the characteristic E_2 and A_1 modes from the GaN substrate. To reveal the crystalline quality of as-grown WS_2 on GaN, the PL spectra are measured and shown in Fig. 1(c). The typical emission band can be deconvoluted into three Lorentzian peaks centered at 629.3, 642.7, and 656.4 nm, respectively, corresponding to the X_A^0 (neutral exciton), X_A^- (negative trion), and LS (localized states) components [37,38]. The LS and X_A^- peaks probably are induced by shadow impurities, defects, or other disorder effects. The X_A^0 peak is much stronger, with a narrow full width at half maximum (FWHM) of 24 nm, indicating the high crystalline quality of the samples. The multilayer area composed of ML, BL, TL, and FL WS_2 on the GaN substrate is imaged by STM, as shown in Fig. 1(d), where the height profile along the black dashed line is displayed in Fig. 1(e). The measured step heights of the second, third, and fourth layers are all ∼0.7 nm, consistent with the expected interlayer spacing of the bulk WS_2 crystal. Due to the different interfacial interaction as well as different contributions of electronic states from GaN and WS_2, the first layer exhibits a larger height value of 1.1 nm [39].

An atomic-resolved STM image of ML WS_2 [Fig. 1(f)] shows a long-range ordered 2D lattice with a honeycomblike structure. The lattice constant of 3.15 Å is deduced from the corresponding hexagonally arranged 2D fast Fourier transform (FFT) spots, which is consistent with previous reports [28]. The inhomogeneous contrast in the electronic morphology of ML WS_2 is attributed to the dielectric disorder in the heterogeneous interface, which is discussed further later. The STS results obtained on the GaN surface and the ML WS_2/GaN heterostructure area are shown in Fig. 1(g). The valence band maximum (VBM) and conduction band minimum (CBM), denoted by the black dashed lines, located at -1.57 ± 0.05 and 1.35 ± 0.05 eV for the GaN surface, respectively, corresponding to a quasi-particle band gap of 2.92 ± 0.10 eV. The band-gap value is slightly smaller than that of bulk GaN because of the presence of dangling bonds in the surface. When forming the WS_2/GaN heterostructure, the CBM of GaN slightly downshifts to 1.25 ± 0.05 eV due to the doping effect from WS_2. However, the measured VBM locates

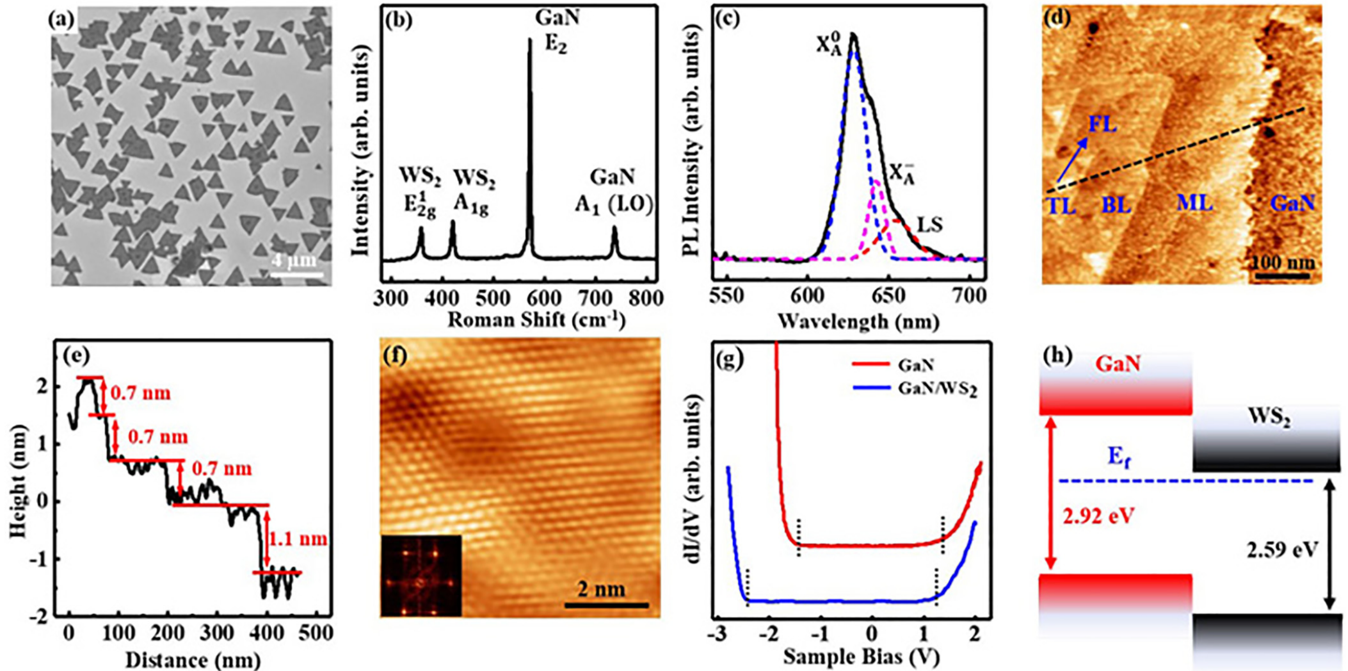

FIG. 1. Morphological and electronic properties of WS_2/GaN heterostructures. (a) SEM image and (b) Raman spectra of GaN/WS_2 heterostructures. (c) PL spectrum of ML WS_2 on GaN. (d) High-resolution STM image of multilayer WS_2 on GaN and (e) the height profile along the black dashed line in (d). (f) Atomic-resolved STM image of ML WS_2 on GaN. (g) Normalized STS spectra of GaN and ML WS_2/GaN heterostructure. (h) Proposed band alignment of WS_2/GaN heterostructure.

at –2.48 ± 0.05 eV, which is far away from the original VBM position of GaN, implying that the VBM of the ML WS_2/GaN heterostructure originated from WS_2. Moreover, according to the reported band-gap value of ML WS_2 (2.59 eV) [40], the CBM of WS_2 should locate at 0.11 ± 0.05 eV. Since the Fermi level presents at ∼2.48 eV above the VBM, the WS_2 film is determined to be n−doped. According to the analysis, the band alignment of the heterostructure is speculated to be a typical type II configuration, as shown in Fig. 1(h).

To explore the inhomogeneous electronic structures [Fig. 1(f)] of the ML WS_2/GaN heterostructure, we systematically measure a series of dI/dV spectra on various positions of WS_2 with a fine step of 0.5 nm. Figure 2(b) is the color rendering of the band mapping along the black dashed lines in Fig. 2(a), where the numbers on the spectra correspond to their positions in the STM image. Some typical dI/dV spectra are provided in Supplemental Material Fig. S2(a) [33]. The CBM originated from the GaN substrate is mostly pinned at a stable position for all measured positions. The position of VBM gradually varies from –2.72 ± 0.05 eV to –1.60 ± 0.05 eV, corresponding to a large upshift of 1.12 eV, implying that the electronic structure of ML WS_2 is strongly modified by the GaN substrate.

Moving into the BL WS_2 region [Fig. 2(c)], the surface becomes more homogeneous and smoother compared with that of the ML region [Fig. 2(a)]. Spatially resolved STS measurements are carried out every 0.7 nm in this region, with the corresponding color rendering of band mapping shown in Fig. 2(d) and typical dI/dV spectra shown in Supplemental Material Fig. S2(b) [33]. The signal of CBM of the BL WS_2/GaN heterostructure is weaker than that of the ML WS_2/GaN due to the larger tunneling distance between GaN and the tip. Furthermore, different from the ML WS_2/GaN heterostructure, the VBM of BL WS_2/GaN is located around −2.17 eV, with an energy fluctuation of 0.20 eV, implying that the second-layer WS_2 withstands a slight regulation effect by the GaN substrate.

To confirm further the different modulations from GaN, the PL mapping image is acquired on the coexisting region of ML and BL WS_2. As shown in Fig. 2(e), the large-triangle WS_2 is composed of a ML domain with a BL center. Due to the transition from a direct (ML WS_2) to an indirect (BL WS_2) band gap, the BL region exhibits as a dim triangular shape, with the integrated intensity weaker than that of the ML [41]. Typical PL spectra of the ML and BL WS_2/GaN heterostructures are shown in Supplemental Material Fig. S2(c) [33]. The PL intensity of the ML area shows a considerable fluctuation, while that all over the BL area illustrates a more homogeneous distribution, which is consistent with the results of our STS measurements. The FWHM of the PL signal is summarized as a histogram for ML and BL WS_2 in Fig. 2(f). The FWHM value changes from 12.8 to 18.3 nm for ML WS_2, revealing a huge fluctuation of 5.5 nm, but shows only a slight change from 14.4 to 15.4 nm for BL WS_2. This indicates that the GaN substrate can effectively impact the electronic properties of ML WS_2, but has weak influence on that of BL WS_2.

In general, the corrugation of the WS_2/GaN interface modifies the electronic properties of WS_2 by two dominated mechanisms: strain fluctuation and dielectric effect. For the former, the strain of WS_2 on the GaN surface is estimated by employing circular fitting from the height profile and analyzing the lattice deformation from the FFT image, respectively.

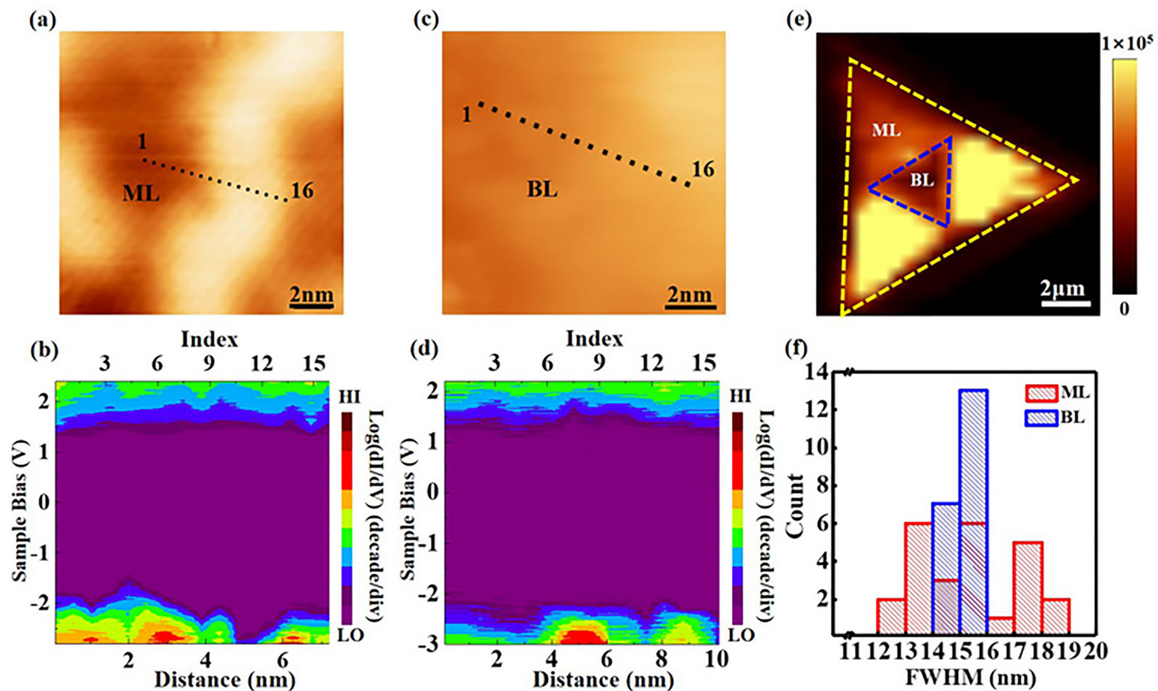

FIG. 2. Characterizations of electronic structures in the ML and BL WS_2/GaN heterostructures by STS and PL measurements. (a, c) STM image and (b, d) STS spectra of ML and BL WS_2 on GaN taken along the path shown in (a) and (c), respectively. The spectra numbers are labeled from left to right (black dashed lines). The color rendering of band mappings is plotted in terms of $\log(dI/dV)$. (e) PL mapping of the coexisting regions of ML and BL WS_2. (f) Statistics of the PL FWHM of ML and BL WS_2.

As seen in Supplemental Material Fig. S3 [33], the statistical results show that the local strain of WS_2 film mostly locates in the range from –1.8% to 1.8%. According to the DFT calculations for the band structures of ML WS_2 under $\pm1.8\%$ strain, the VBM and band gap show the variations of 0.03 and 0.28 eV, respectively (Supplemental Material Fig. S4 [33]). There results indicate that the strain has a small contribution to the change in the band structure of WS_2/GaN heterostructures. Therefore, the strain fluctuation is not considered as a dominant factor modulating the electronic properties of WS_2/GaN heterostructures. On the contrary, dielectric disorder originating entirely from local fluctuations of the environmental permittivity can intensively influence the Coulomb interaction in 2D materials, and thus affect their local physical properties, such as band structure and exciton states [18]. The surface corrugation of the WS_2/GaN heterostructure is measured as $\sim$0.3 nm under different bias voltages, as shown in Supplemental Material Fig. S5 [33]. The spatial fluctuation combined with the large polarization field in the GaN surface is enough to change the external dielectric environment and induce inhomogeneous electronic states in ML WS_2. It has been reported that a successful encapsulation for 2D materials can effectively mitigate the effect of the dielectric disorder [18,19]. Hence, the weak dielectric effect on the second-layer WS_2 can be attributed to the shielding of the first-layer WS_2 from the GaN substrate.

In order to demonstrate the shielding effect of ML WS_2 for dielectric disorder, the electronic structures of TL WS_2/GaN and FL WS_2/GaN heterostructures are further investigated. Figure 3(a) is a close-up STM image of a coexisting region of the TL and FL WS_2. The black dashed line crossing the

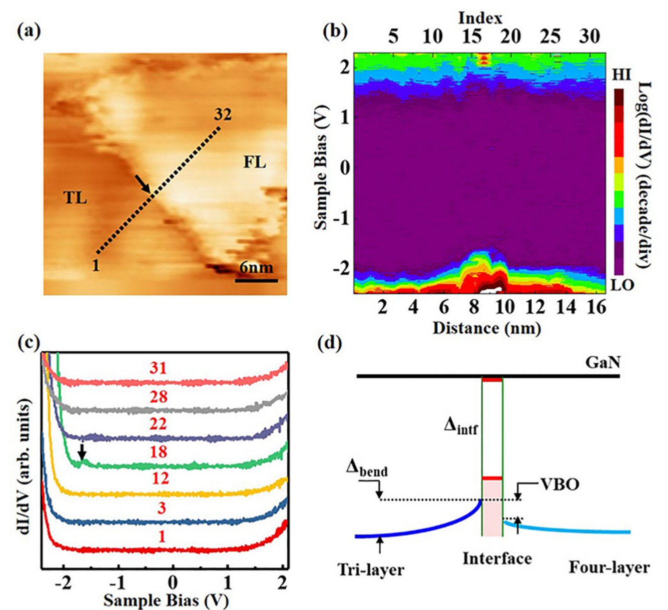

FIG. 3. STS investigation of band diagram across the TL and FL WS_2/GaN heterostructures. (a) The close-up STM image of TL and FL WS_2 on the GaN substrate, where the black dashed line shows the path that the STS spectra are taken. (b) Color rendering and (c) typical dI/dV spectra from the band mapping of the TL and FL WS_2/GaN heterostructures, where the edge states are marked in spectrum #18. (d) Schematic diagram showing the band alignment of the TL and FL WS_2/GaN heterostructures, where Δ_{bend}, Δ_{intf}, and VBO denote the band bending, band gap of the interface, and the valence band offset, respectively.

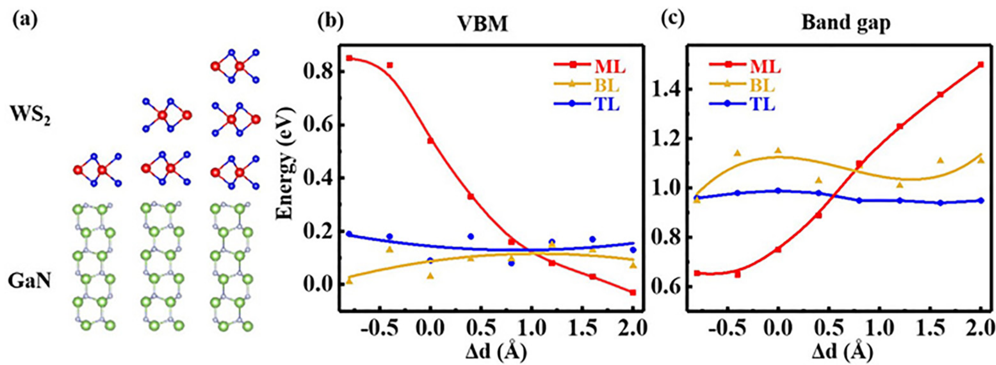

FIG. 4. Simulated geometrical configurations and band structure variations of WS_2/GaN heterostructures by the first-principles calculations. (a) Geometrical structures of the ML, BL, and TL WS_2/GaN heterostructures. (b) The VBM and (c) band gap of ML, BL, and TL WS_2 as a function of the interfacial distance variation between GaN and WS_2.

two regions illustrates the spatial positions where the band mapping was carried out. The color rendering of the band mapping and representative STS curves are displayed in Fig. 3(b) and 3(c), respectively. Far away from the edge (spectra from #1 to #9), between TL and FL WS_2, the VBM of TL WS_2 is pinned at 2.02 ± 0.05 eV, which indicates that the interface dielectric disorder effect is essentially eliminated. As one approaches the edge (spectra from #10 to #15), the VBM upshifts 0.20 ± 0.05 eV, corresponding to the band bending [42]. An ultra-short depletion length of about 2.3 nm is observed in the edge, which can be attributed to the heavy n−type doping of WS_2 (the Fermi level located at 2.02 eV above the VBM) [43]. Right at the edge of FL WS_2, a prominent peak around −1.6 eV is present in the valence band, especially for spectrum #18 (marked by the black arrow). As revealed by the STS mapping, the interface states induce a distinct upshift for about 0.4 eV at VBM comparing with that of the TL WS_2. The localized interface states are derived from the existence of edge dangling bonds [42], and can act as confined quantum wires for hole transport. Moving into the FL WS_2 region, the VBM is higher than that of the TL WS_2 due to the stronger interlayer interaction. Meanwhile, the position of the VBM is relatively stable, at ∼1.95 eV, except for a slight band bending induced by the interface states, similar to the results in the TL WS_2 region. The band alignment and interface behavior of the lateral heterostructure formed by TL and FL WS_2 are summarized in the schematic diagram in Fig. 3(d). The band bending, band gap of the interface, and the valence band offset (VBO) are measured as ∼0.2, 2.92, and 0.1 eV, respectively.

To elaborate the physical mechanism of the dielectric modulation effect on WS_2, first-principles calculations are performed. All possible stacking configurations are designed for the ML, BL, and TL WS_2/GaN heterostructures, as seen in Supplemental Material Figs. S6 and S7 [33]. Based on the binding energies, the three most stable configurations of the heterostructures are revealed and shown in Fig. 4(a). The corrugation of the GaN surface results in a local change of interfacial distance, which induces the fluctuation of the external dielectric environment. To simulate the dielectric effect, the band structures under different interfacial distances are calculated for the ML, BL, and TL WS_2/GaN heterostructures (Supplemental Material Fig. S8 [33]). Accordingly, the VBM positions and the band gaps of top-layer WS_2 are extracted, and their dependence on the interfacial distance is shown in Fig. 4(b) and (4(c)). The optimized interfacial distance of the ML, BL, and TL WS_2/GaN heterostructures are 2.53, 2.49, and 2.48 Å, respectively. When the variation of the interfacial distance changes from −0.8 to 2.0 Å, the VBM of ML WS_2 shows a dramatic decrease of 0.88 eV. Due to shielding by the first-layer WS_2, the VBM of WS_2 essentially remains stable, with a small fluctuation of 0.14 eV for the second layer. As for the TL WS_2/GaN heterostructure, the VBM shows only a slight fluctuation of ∼0.10 eV, implying a negligible dielectric disorder effect, which agrees well with the STS measurements. Simultaneously, with the decrease in the interfacial distance, the band gap is reduced from 1.50 to 0.65 eV. This is ascribed to the suppressed electron-electron Coulomb interactions in ML WS_2 owing to the dielectric effect of the substrate. In contrast, the band gap of the second layer exhibits a slight fluctuation of 0.10 eV around the value of 1.03 eV, and the third-layer WS_2 almost remains stable at about 0.98 eV with the change in the interfacial distance. Note that DFT calculations typically underestimate the band gap values; however, the band dispersion as well as the evolution trend of the electronic structure of WS_2 are still valid [5,44]. To analyze the modulation effect of the possible reconstructed GaN surface on the electronic structure of WS_2, the band structures under different interfacial distances are calculated for heterostructures between WS_2 and the 1×1 reconstructed GaN surface, as shown in Supplemental Material Fig. S9 [33]. The results suggest that the layer-dependent dielectric modulation effect also can be extended to the reconstructed GaN surface.

Essentially, redistribution of the charge and the electrostatic potential in the heterogeneous interface are responsible for the modulation of the dielectric environment. Differential charge densities, electrostatic potential energy, and charge transfer are calculated and shown in Fig. 5. For the optimized stacking structures, lots of charge accumulates in the interface, implying a strong interaction between GaN and WS_2. At the equilibrium interfacial distance, the electrostatic potentials exhibit periodic variation in WS_2 and GaN, and the

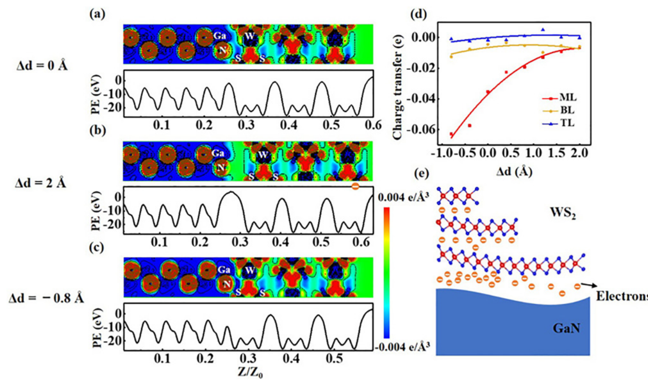

FIG. 5. Simulated differential charge densities, electrostatic potential energies, and charge transfer of WS_2/GaN heterostructures by first-principles calculations. (a)–(c) Differential charge densities of the (110) plane and the electrostatic potential energy (PE) of WS_2/GaN heterostructures with different interfacial distances. (d) Interfacial charge transfer in the ML, BL, and TL WS_2/GaN heterostructures as a function of the interfacial distance between GaN and WS_2. (e) A schematic diagram of the dielectric modulation effect in WS_2/GaN heterostructures.

values are basically comparable in the interface, as shown in Fig. 5(a). When increasing the interfacial distance by 2.0 Å, the interaction between GaN and ML WS_2 becomes weak, resulting in a decrease of the charge transfer from ML WS_2 to GaN, as shown in Fig. 5(d). The accumulated charge at the heterogeneous interface also decreases, as shown in Fig. 5(b). Hence, the electrostatic potential in the interface is significantly increased, so as to isolate the influence of electrostatic field of the GaN surface on WS_2, and the Coulomb interaction between electrons in the first-layer WS_2 is enhanced. When decreasing the interfacial distance, all the previous evolution tendencies reverse. An atomic-level steep dielectric polarization field is formed at the interface between GaN and WS_2, as shown in Fig. 5(c). Consequently, the Coulomb interaction between electrons in WS_2 is suppressed, and the band gap of ML WS_2 decreases. Interestingly, under the screening protection of the first-layer WS_2, the charge distribution and transfer of the second- and third-layer WS_2 almost remain stable with the change of interfacial distance, consistent with previous results. As the physical mechanism is revealed, the schematic diagram of dielectric modulation effect is depicted in Fig. 5(e).

IV. CONCLUSION

Two-dimensional WS_2 with multilayer thickness is grown on a GaN substrate through the CVD method, and layer-dependent dielectric modulation of their electronic structures is studied by combining STM, PL, and first-principles calculations. The results show that the dielectric environment fluctuations induced by local corrugation of the GaN surface have the ability to control the Coulomb interaction within ML WS_2. As a result, the electronic structure of the system is dramatically modulated, where the VBM shows a large downshift of 1.12 eV. However, under the shielding of the first-layer WS_2, the dielectric environment shows a weak modulation effect on the second layer, and even has negligible influence on the third and fourth layers. The relationship between the dielectric environment and the interfacial distance is further simulated by first-principles calculations. When increasing the interfacial distance, weaker interfacial interaction results in a downshift of VBM energy and an increase in the band gap. When decreasing the interfacial distance, all the previous evolution tendencies reverse. The electrostatic potential energy, differential charge densities, and charge transfer of WS_2/GaN heterostructures under different interfacial distances reveal that the differences of charge redistributions between the WS_2/GaN interface and the WS_2 interlayer are responsible for layer-dependent dielectric modulation. Our findings provide an unprecedented understanding of many-electron physics in WS_2/GaN heterostructures and pave the way toward the creation of next-generation 2D nanodevices.

ACKNOWLEDGMENTS

This work was funded by the National Key Research and Development Program of China (Grant No. 2022YFB3605604), the National Science Fund for Excellent Young Scholars (Grant No. 62022068), the National Natural Science Foundation of China (Grants No. 61974123, No. 61874092, No. 62274139, and No. 61804129), and the Science and Technology Project of Fujian Province of China (Grant No. 2019H0002).

[1] F. Capasso, Band-gap engineering: From physics and materials to new semiconductor devices, Science **235**, 172 (1987).

[2] Z. Z. Qiu *et al.*, Giant gate-tunable bandgap renormalization and excitonic effects in a 2D semiconductor, Sci. Adv. **5**, eaaw2347 (2019).

[3] M. M. Ugeda, A. J. Bradley, S.- F. Shi, F. H. da Jornada, Y. Z. Zhang, D. Y. Qui, W. Ruan, S.- K. Mo, Z. Hussain, Z.- X. Shen, F. Wang, S. G. Louie, and M. F. Crommie. Giant bandgap renormalization and excitonic effects in a monolayer transition metal dichalcogenide semiconductor, Nat. Mater. **13**, 1091 (2014).

[4] K. He, N. Kumar, L. Zhao, Z. Wang, K. F. Mak, H. Zhao, and J. Shan, Tightly Bound Excitons in Monolayer WSe_2, Phys. Rev. Lett. **113**, 026803 (2014).

[5] H. P. Komsa and A. V. Krasheninnikov, Effects of confinement and environment on the electronic structure and exciton binding energy of MoS_2 from first principles, Phys. Rev. B. **86**, 241201(R) (2012).

[6] D. Y. Qiu, H. Felipe, and S. G. Louie, Optical Spectrum of MoS_2: Many-body Effects and Diversity Of Exciton States, Phys. Rev. Lett. **111**, 216805 (2013).

[7] A. Chernikov, T. C. Berkelbach, H. M. Hill, A. Rigosi, Y. Li, B. Aslan, D. R. Reichman, M. S. Hybertsen, and T. F. Heinz. Exciton Binding Energy and Nonhydrogenic Rydberg Series in Monolayer WS_2, Phys. Rev. Lett. **113**, 076802 (2014).

[8] A. Raja, A. Chaves, J. Yu, G. Arefe, H. M. Hill, A. F. Rigosi, T. C. Berkelbach, P. Nagler, C. Schüller, T. Korn, C. Nuckolls, J. Hone, L. E. Brus, T. F. Heinz, D. R. Reichman, and A.

Chernikov. Coulomb engineering of the bandgap and excitons in two-dimensional materials, Nat. Commun. **8**, 15251 (2017).

[9] Y. Lin, X. Ling, L. Yu, S. Huang, A. L. Hsu, Y. H. Lee, J. Kong, M. S. Dresselhaus, and T. Palacios, Dielectric screening of excitons and trions in single-layer MoS_2, Nano Lett. **14**, 5569 (2014).

[10] K. Andersen, S. Latini, and K. S. Thygesen, Dielectric genome of van der Waals heterostructures, Nano Lett. **15**, 4616 (2015).

[11] S. Latini, T. Olsen, and K. S. Thygesen, Excitons in van der Waals heterostructures: The important role of dielectric screening, Phys. Rev. B **92**, 245123 (2015).

[12] M. Rosner, C. Steinke, M. Lorke, C. Gies, F. Jahnke, and T. O. Wehling, Two-dimensional heterojunctions from nonlocal manipulations of the interactions, Nano Lett. **16**, 2322 (2016).

[13] M. L. Trolle, T. G. Pedersen, and V. Véniard, Model dielectric function for 2D semiconductors including substrate screening, Sci. Rep. **7**, 39844 (2017).

[14] A. V. Stier, N. P. Wilson, G. Clark, X. Xu, and S. A. Crooker, Probing the influence of dielectric environment on excitons in monolayer WSe_2: Insight from high magnetic fields, Nano Lett. **16**, 7054 (2016).

[15] M. I. B. Utama, H. Kleemann, W. Zhao, C. S. Ong, F. H. da Jornada, D. Y. Qui, H. Cai, H. Li, R. Kou, S. Zhao, S. Wang, K. Watanabe, T. Taniguchi, S. Tongay, A. Zettl, S. G. Louie, and F. Wang. A dielectric-defined lateral heterojunction in a monolayer semiconductor, Nat. Electron. **2**, 60 (2019).

[16] W. Q. Tang, C. M. Ke, K. Chen, Z. M. Wu, Y. P. Wu, X. Li, and J. Y. Kang, Magnetism manipulation of Co n-adsorbed monolayer WS_2 through charge injection, J. Phys.: Condens. Matter **32**, 275001 (2020).

[17] A. J. Bradley, M. M. Ugeda, D. F. H. Jornada, D. Y. Qiu, W. Ruan, Y. Zhang, S. Wickenburg, A. Riss, J. Lu, and S. K. Mo, Probing the role of interlayer coupling and coulomb interactions on electronic structure in few-layer $MoSe_2$ nanostructures, Nano Lett. **15**, 2594 (2015).

[18] A. Raja, L. Waldecker, J. Zipfel, Y. Cho, S. Brem, J. D. Ziegler, M. Kulig, T. Taniguchi, K. Watanabe, and E. Malic, Dielectric disorder in two-dimensional materials, Nat. Nanotechnol. **14**, 832 (2019).

[19] X. Cui, G. H. Lee, Y. D. Kim, G. Arefe, P. Y. Huang, C.- H. Lee, D. A. Chenet, X. Zhang, L. Wang, F. Ye, F. Pizzocchero, B. S. Jessen, K. Watanabe, T. Taniguchi, D. A. Muller, T. Low, P. Kim, and J. Hone. Multi-terminal transport measurements of MoS_2 using a van der Waals heterostructure device platform, Nat. Nanotechnol. **10**, 534 (2015).

[20] C. Zhou, W. Yang, and H. Zhu, Mechanism of charge transfer and its impacts on Fermi-level pinning for gas molecules adsorbed on monolayer WS_2, J. Chem. Phys. **142**, 214704 (2015).

[21] B. Liu, W. Zhao, Z. Ding, I. Verzhbitskiy, L. Li, J. Lu, J. Chen, G. Eda, and K. P. Loh. Engineering bandgaps of monolayer MoS_2 and WS_2 on fluoropolymer substrates by electrostatically tuned many-body effects, Adv. Mater. **28**, 6457 (2016).

[22] F. Cadiz, E. Courtade, C. Robert, G. Wang, Y. Shen, H. Cai, T. Taniguchi, K. Watanabe, H. Carrere, D. Lagarde, M. Manca, T. Amand, P. Renucci, S. Tongay, X. Marie, and B. Urbaszek. Excitonic Linewidth Approaching The Homogeneous Limit in MoS_2−based Van Der Waals Heterostructures, Phys. Rev. X **7**, 021026 (2017).

[23] G. Wang, A. Chernikov, M. M. Glazov, T. F. Heinz, X. Marie, T. Amand, and B. Urbaszek, Colloquium: Excitons in atomically thin transition metal dichalcogenides, Rev. Mod. Phys. **90**, 021001 (2018).

[24] Y. C. Pu, M. Kibria, Z. Mi, and J. Z. Zhang, Ultrafast exciton dynamics in InGaN/GaN and Rh/Cr_2O_3 nanoparticle-decorated InGaN/GaN nanowires, J. Phys. Chem. Lett. **6**, 2649 (2015).

[25] A. Khan, K. Balakrishnan, and T. Katona, Ultraviolet light-emitting diodes based on group three nitrides, Nat. Photon. **2**, 77 (2008).

[26] Y. Wan, J. Xiao, J. Li, X. Fang, K. Zhang, L. Fu, P. Li, Z. Song, H. Zhang, Y. Wang, M. Zhao, J. Lu, N. Tang, G. Ran, X. Zhang, Y. Ye, and L. Dai. Epitaxial single-layer MoS_2 on GaN with enhanced valley helicity, Adv. Mater. **30**, 1703888 (2018).

[27] Z. M. Wu, H. Zeng, W. Q. Tang, C. M. Ke, Y. P. Wu, X. Li, and J. Y. Kang, Enormous valley splitting in monolayer WS_2 by coupling with an N-terminated GaN substrate, Phys. Status Solidi **15**, 2000493 (2021).

[28] J. Chen, K. Shao, W. Yang, W. Tang, J. Zhou, Q. He, Y. Wu, C. Zhang, X. Li, X. Yang, Z. Wu, and J. Kang. Synthesis of wafer-scale monolayer WS_2 crystals toward the application in integrated electronic devices, ACS Appl. Mater. Interfaces **11**, 19381 (2019).

[29] W. Tang, M. Fu, J. Chen, B. Sun, C. Ke, Y. Wu, X. Li, C. Zhang, Z. Wu, and J. Kang. Identically Sized Co Quantum Dots on Monolayer WS_2 Featuring Ohmic Contact, Phys. Rev. Appl. **13**, 024003 (2020).

[30] G. Kresse and J. Hafner, Ab initio molecular-dynamics simulation of the liquid-metal-amorphous-semiconductor transition in germanium, Phys. Rev. B **49**, 14251 (1994).

[31] J. P. Perdew, K. Burke, and M. Ernzerhof, Generalized Gradient Approximation Made Simple, Phys. Rev. Lett. **77**, 3865 (1996).

[32] W. Q. Tang, X. F. Wu, Y. P. Wu, Z. M. Wu, S. P. Li, and J. Y. Kang, Controllable enormous valley splitting in Janus WSSe on CrN monolayer, J. Phys. D: Appl. Phys. **54**, 425304 (2021).

[33] See Supplemental Material at http://link.aps.org/supplemental/10.1103/PhysRevB.107.085304 for the surface features of GaN, typical dI/dV and PL spectra of the ML and BL WS_2/GaN heterostructures, the influence of strain on the band structure of WS_2/GaN heterostructures, morphology characterization of WS_2/GaN heterostructures, possible geometrical structures of WS_2/GaN heterostructures, and band structures of WS_2/GaN heterostructures calculated by first-principles calculations.

[34] S. W. Kaun, P. G. Burke, M. H. Wong, E. C. H. Kyle, U. K. Mishra, and J. S. Speck. Effect of dislocations on electron mobility in AlGaN/GaN and AlGaN/AlN/GaN heterostructures, Appl. Phys. Lett. **101**, 262102 (2012).

[35] W. Luo, B. Liu, Z. Li, L. Li, Q. Yang, L. Pan, C. Li, D. Zhang, X. Dong, D. Peng, F. Yang, and R. Zhang. Enhanced p-type conduction in AlGaN grown by metal-source flow-rate modulation epitaxy, Appl. Phys. Lett. **113**, 072107 (2018).

[36] H. R. Gutiérrez, N. Perea-López, A. L. Elías, A. Berkdemir, B. Wang, R. Lv, F. López-Urías, V. H. Crespi, H. Terrones, and M. Terrones. Extraordinary room-temperature photoluminescence in triangular WS_2 monolayers, Nano Lett. **13**, 3447 (2013).

[37] Y. Sheng, H. Tan, X. Wang, and J. H. Warner, Hydrogen addition for centimeter-sized monolayer tungsten disulfide continuous films by ambient pressure chemical vapor deposition, Chem. Mater. **29**, 4904 (2017).

[38] J. Shang, X. Shen, C. Cong, N. Peimyoo, B. Cao, M. Eginlligil, and T. Yu. Observation of excitonic fine structure in a

2D transition-metal dichalcogenide semiconductor, ACS Nano **9**, 647 (2015).

[39] W. Yan, L. Meng, Z. Meng, Y. Weng, L. Kang, and X. A. Li, Probing angle-dependent interlayer coupling in twisted bilayer WS_2, J. Phys. Chem. C **123**, 30684 (2019).

[40] R. Kumar, I. Verzhbitskiy, F. Giustiniano, T. P. Sidiropoulos, R. F. Oulton, and G. Eda, Interlayer screening effects in WS_2/WSe_2 van der Waals hetero-bilayer, 2D Mater. **5**, 041003 (2018).

[41] Y. Guo, X. Fu, and Z. Peng, Controllable synthesis of MoS_2 nanostructures from monolayer flakes, few-layer pyramids to multilayer blocks by catalyst-assisted thermal evaporation, J. Mater. Sci. **53**, 8098 (2018).

[42] C. Zhang, Y. Chen, J. K. Huang, X. Wu, L. J. Li, W. Yao, J. Tersoff, and C. K. Shih, Visualizing band offsets and edge states in bilayer-monolayer transition metal dichalcogenides lateral heterojunction, Nat. Commun. **7**, 10349 (2016).

[43] C. Zhang, A. Johnson, C. L. Hsu, L. J. Li, and C. K. Shih, Direct imaging of band profile in single layer MoS_2 on graphite: Quasiparticle energy gap, metallic edge states, and edge band bending, Nano Lett. **14**, 2443 (2014).

[44] B. G. Shin, G. H. Han, S. J. Yun, H. M. Oh, J. J. Bae, Y. J. Song, C.- Y. Park, and Y. H. Lee. Indirect bandgap puddles in monolayer MoS_2 by substrate-induced local strain, Adv. Mater. **28**, 9378 (2016).